Quality Assessment of Weather Radar Wind Profiles during Bird Migration

IWAN HOLLEMAN

Royal Netherlands Meteorological Institute (KNMI), De Bilt, Netherlands

HANS VAN GASTEREN

Institute for Biodiversity and Ecosystem Dynamics, Universiteit van Amsterdam, Amsterdam, and Royal Netherlands Air Force (RNLAF), Breda, Netherlands

WILLEM BOUTEN

Institute for Biodiversity and Ecosystem Dynamics, Universiteit van Amsterdam, Amsterdam, Netherlands

ABSTRACT

Wind profiles from an operational C-band Doppler radar have been combined with data from a bird tracking radar to assess the wind profile quality during bird migration. The weather radar wind profiles (WRWPs) are retrieved using the well-known volume velocity processing (VVP) technique. The X-band bird radar performed range–height scans perpendicular to the main migration direction and bird densities were deduced by counting and normalizing the observed echoes. It is found that the radial velocity standard deviation (σ_r) obtained from the VVP retrieval is a skillful indicator of bird migration. Using a threshold of 2 m s^{-1} on σ_r, more than 93% of the bird-contaminated wind vectors are rejected while over 70% of the true wind vectors are accepted correctly. For high bird migration densities the raw weather radar wind vectors have a positive speed bias of 8.6 ± 3.8 m s^{-1}, while the quality-controlled wind vectors have a negligible speed bias. From the performance statistics against a limited area numerical weather prediction model, it is concluded that all (significant) bird contamination is removed and that high-quality weather radar wind profiles can be obtained, even during the bird migration season.

1. Introduction

Weather radar wind profiles (WRWPs) are used increasingly to improve operational numerical weather prediction (NWP) models. Zhao et al. (2006) have assimilated radial velocity data from three Weather Surveillance Radar-1988 Doppler (WSR-88D) sites on the East Coast in a mesoscale NWP model. They conclude that "radar observations contain valuable information about the mesoscale and storm-scale structures of the atmosphere and hydrometeors with high spatial resolutions and frequent update rate, and therefore have the potential to become a major data source for high-resolution NWP model initialization." The four-dimensional variational data assimilation (4DVAR) radar data analysis system for low-level wind and temperature retrieval of Sun and Crook (2001) has run at a single WSR-88D radar for two summers. During the Sydney 2000 Forecast Demonstration Project, this system was also used to analyze and forecast the low-level wind (Crook and Sun 2004). For strong gust front cases these forecasts improved over persistence up to 1 h ahead. Assimilation of Doppler radar wind data over northern Europe in the High-Resolution Limited-Area Model (HIRLAM) with 3DVAR has been reported by Lindskog et al. (2004). Improved forecasts of wind and temperature in the low and middle troposphere are found at 22-km horizontal resolution. These improvements are seen for both weather radar wind profiles and radial velocity data.

Rinne (2000) presents an overview of the problems and consequences of using radar wind observations in NWP assimilation. He underlines the need for removal

Corresponding author address: I. Holleman, Royal Netherlands Meteorological Institute, P.O. Box 201, NL-3730 AE De Bilt, Netherlands.
E-mail: holleman@knmi.nl

of erroneous data (e.g., due to migrating birds or velocity aliasing). Assimilation of wind profiles from ten WSR-88D sites in summertime meteorological simulations is described by Michelson and Seaman (2000). A sophisticated quality-check filter to identify and eliminate unreliable wind profile data before assimilation was a prerequisite for obtaining good results. Collins (2001) has reported on the operational assimilation of WSR-88D wind profiles at the National Centers for Environmental Prediction (NCEP) from July 1997 to January 1999. The operational assimilation was ended because of many problems with data quality (i.e., random errors, ground clutter, gross errors, and migrating birds). A quality-control technique was developed to identify these errors (Collins 2001). In Europe the quality of weather radar wind profiles is monitored centrally (Parrett et al. 2004). Although the quality of most wind profile data is comparable to that of radiosondes, speed and direction biases are sometimes seen, especially at low levels.

Boundary layer clear-air weather radar echoes are mainly due to insects and migrating birds (Wilson et al. 1994; Martin and Shapiro 2007). Gauthreaux and Belser (1998) have studied bird movements on the WSR-88D displays, identified patterns, and extracted quantitative information. The ground speeds of migrating birds may exceed wind speeds by more than 12.9 m s^{-1} and thus can seriously inflate winds measured with Doppler surveillance radars (Gauthreaux et al. 1998). Koistinen (2000) has extensively studied bird migration patterns on the Finnish weather radars. He concludes that the major part of the bird migration is so weak in reflectivity that no significant effects on the accumulated precipitation products are to be expected, but that detection and elimination of migrating birds from Doppler data for use in NWP assimilation is definitely needed. A two-step procedure for (i) extraction of bird migration features from Doppler velocity images (Zhang et al. 2005) and (ii) probabilistic identification and quality control of contaminated data has been developed (Liu et al. 2005), but further evaluations for different seasons and regions are required. In a previous study, which was not focused on bird contamination, Holleman (2005) describes a quality control of weather radar wind profiles and presents an extensive verification over a 9-month period, including the autumn and spring migration seasons. Interestingly, the observation minus NWP background statistics of these wind profiles were at least as good as those of the radiosonde profiles. In this comparison, the radiosonde had a clear advantage over the weather radar because it is assimilated by the NWP model.

Here we present a quality assessment of weather radar wind profiles during the bird migration of spring 2003 in the Netherlands using data from a bird tracking radar. A brief review of the wind profile retrieval algorithm and a detailed description of the X-band bird tracking radar and the spring 2003 dataset are given. Subsequently, the behavior of the mean reflectivity and the radial velocity standard deviation as determined during the wind profile retrieval is investigated. Using so-called contingency tables and derived scores, it is shown that the standard deviation of the radial velocity is a skillful indicator of bird migration and that it can be used for quality controlling the wind profiles. The speed bias of the radar wind profiles with/without quality control against the profiles from the HIRLAM NWP model is discussed as well. Finally, the "observation minus background" statistics of the weather radar against the HIRLAM model during the bird migration season are highlighted and conclusions are drawn. The use of this dataset for the extraction of bird migration information from C-band weather radars is published elsewhere (van Gasteren et al. 2008).

2. Available datasets

a. Wind profiles from weather radar

The Royal Netherlands Meteorological Institute (KNMI) operates two identical C-band Doppler weather radars from SELEX-SI (Meteor 360AC). One weather radar is located in De Bilt (52.10°N, 5.18°E, 40 m above ground level) and the other one is located in Den Helder (52.96°N, 4.79°E, 51 m above ground level). The geographical positions of both Doppler weather radars are indicated on the map in Fig. 1. Data from the weather radar in De Bilt have been used in this study. The radar antennas with a 4.2-m diameter produce a 3-dB beamwidth just below 1°. During Doppler scans the peak power and duration of the transmitted pulses are 300 kW and 0.8 μs, respectively. The dual-PRF technique (750 and 1000 Hz) is used to extend the unambiguous velocity interval up to 40 m s^{-1} (Sirmans et al. 1976; Holleman and Beekhuis 2003). The received signal is digested by an RVP6 radar processor (Sigmet 1998) and the generation of radar products is done with the Rainbow package (Gematronik 2003). Every 15 min a 10-elevation volume scan (0.5°–25°) optimized for profiling up to an altitude of about 6 km is performed. Table 1 lists the relevant technical parameters of the Doppler weather radar.

A Doppler weather radar measures the pulse volume and reflectivity-weighted radial component of the velocity of scatterers. The Doppler weather radar performs a three-dimensional volume scan and thus provides the mean radial velocity as a function of range,
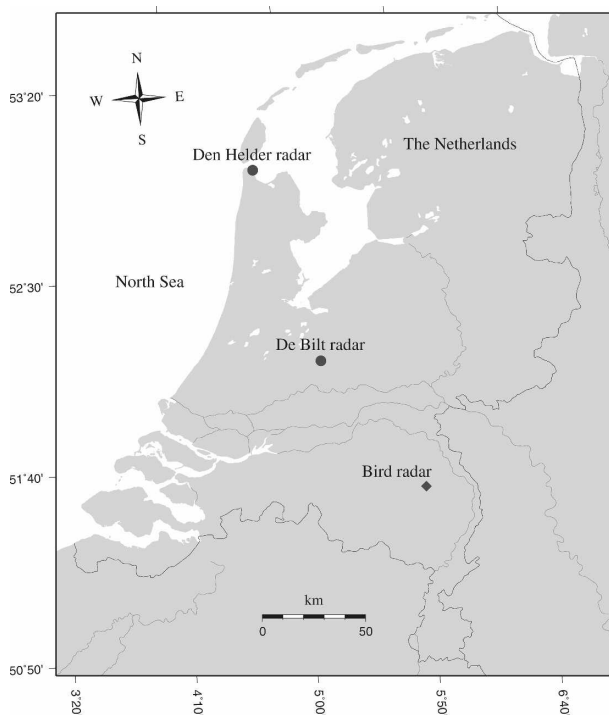
FIG. 1. Map of the Netherlands showing the locations of the operational weather radar in De Bilt and the X-band bird tracking radar at the Air Force Base De Peel.

azimuth, and elevation. Wind profiles can be obtained from single-site radar data under the assumption of a uniform or linear wind model. Using a uniform wind field model (u_0, v_0, w_0) and a constant terminal fall velocity, the radial velocity V_r can be calculated as a function of the beam azimuth ϕ (angle between an-

TABLE 1. Listing of relevant technical parameters of the Doppler weather radar and the X-band bird tracking radar.

| Parameter	Weather radar	Bird radar
Manufacturer	SELEX-SI	Thales group
Radar system	Meteor 360AC	Flycatcher
Geographical position	52.10°N, 5.18°E	51.52°N, 5.85°E
Height above ground level	40 m	28 m
Wavelength	5.33 cm	3.26 cm
Beam diameter	1.0°	2.4°
Pulse peak power	300 kW	160 kW
Pulse duration	0.8 μs	0.2 μs
Pulse repetition frequency	1000/750 Hz	4800 Hz
Range resolution	500 m	30 m
Minimum used range	5 km	2 km
Maximum used range	25 km	4.5 km
Scan type	Azimuth	Elevation
Scanned azimuths	0°–360°	315°
Scanned elevations	0.5°, . . . , 25°	0°–60°
Product generation	Rainbow	ROBIN
Accumulation time	15 min	3 h
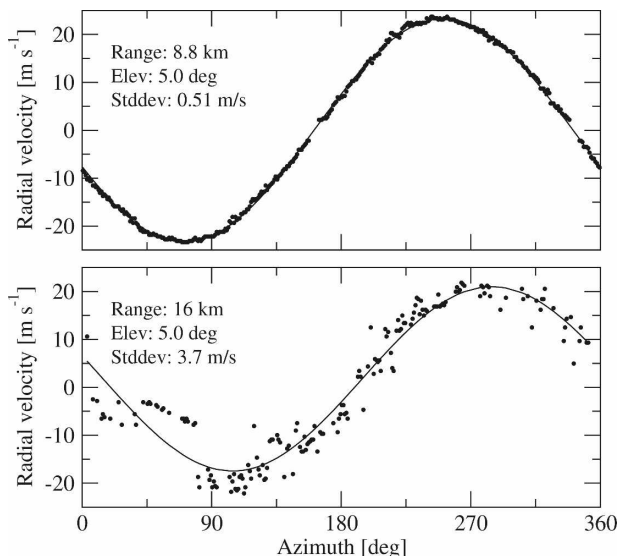
FIG. 2. Two examples of VAD data from the operational weather radar in De Bilt are shown. (top) VAD during the passage of a cold front (1409 UTC 8 Mar 2003) and (bottom) intense bird migration (0009 UTC 7 Mar 2003).

tenna and true north) and elevation θ (angle between antenna and surface):

$$V_r(\phi, \theta) = u_0 \cos\theta \sin\phi + v_0 \cos\theta \cos\phi + w_0' \sin\theta, \quad (1)$$

where w_0' is the sum of the vertical component of the wind and the terminal fall velocity of the hydrometeors. When Doppler data are displayed at constant range and elevation, the radial velocity as a function of azimuth will resemble a sine function (see Fig. 2). The wind speed and direction can be determined from the amplitude and the phase of the sine, respectively. This well-known technique is called velocity–azimuth display (VAD) (Lhermitte and Atlas 1961; Browning and Wexler 1968).

Instead of processing multiple VADs and averaging the results, one can also process all available radial velocity volume data within a certain height layer at once. The parameters of the wind field can then be extracted using a multidimensional and multiparameter linear fit. This so-called volume velocity processing (VVP) technique was introduced by Waldteufel and Corbin (1979). At KNMI the VVP technique is used for the operational production of weather radar wind profiles with a 200-m height resolution. To control the errors due to nonuniformity of the wind field, the analyzed volume is limited by applying a maximum range of 25 km. For each height layer, the mean radar reflectivity is calculated by linear averaging of all reflectivity data measured in the analyzed volume. More details on the VVP

algorithm used in this study can be found in Holleman (2005).

Figure 2 shows two examples of radial velocity data from the operational weather radar in De Bilt. The upper frame displays a high-quality "wind" VAD during the passage of a cold front while the lower frame shows a VAD during intense bird migration. The huge difference in scatter of the observed radial velocity $V_{r,i}$ data around the modeled radial velocities $V_r(\phi_i, \theta_i)$ is evident. The amount of scatter can be quantified using the radial velocity standard deviation. This standard deviation σ_r can be calculated during the wind profile retrieval using the chi-squared merit function (Press et al. 1992):

$$\sigma_r^2 = \frac{1}{N - M} \sum_{i=1}^{N} [V_{r,i} - V_r(\phi_i, \theta_i)]^2, \qquad (2)$$

where $V_{r,i}$ are the observed radial velocities, N is the number of data points, and M is the number of estimated parameters in the radial velocity model [$M = 3$ in Eq. (1)]. Koistinen (2000) has noted that "the rms-difference between a linearly fitted VVP or VAD wind and the individual bin values is larger in bird migration than in rain or insect migration." Alternatively, large differences can occur when the actual wind field is not uniform (e.g., during strong wind shear) or when the terminal fall velocity is not constant (e.g., in a mixture of snow and rain) (Browning and Wexler 1968). KNMI provides both the wind profile data and the retrieved standard deviations σ_r to the users. A default threshold of 2.0 m s^{-1} is suggested to discriminate high-quality and poor-quality wind vectors (Holleman 2005), but the optimum threshold depends on the application.

b. Wind profiles from HIRLAM

The weather radar wind profiles are referenced against wind profiles from the operational NWP model, HIRLAM (Unden et al. 2002). In 2003 the hydrostatic HIRLAM ran at a horizontal resolution of 22 km with 31 vertical levels. Every 3 h the model analyzes the state of the atmosphere. Wind profiles at the grid point nearest to De Bilt (distance 11 km) have been retrieved from the initialized HIRLAM analyses and interpolated to 200-m-thick height layers.

c. Data from X-band bird tracking radar

The bird tracking radar is an X-band Flycatcher tracking radar (Thales group) of the Royal Netherlands Air Force (RNLAF) (Bouten et al. 2003; Shamoun-Baranes et al. 2006). It was located at De Peel Air Force base (51.52°N, 5.85°E, 28 m above ground level),
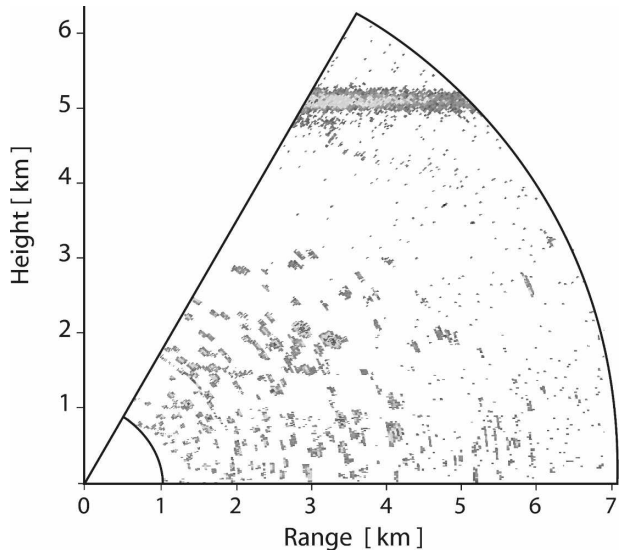

FIG. 3. An example of a range–height scan from the bird tracking radar is shown. This scan has been recorded at an azimuth of 315°, i.e., perpendicular to the main migration direction (northeast). The maximum range and elevation are 7 km and 60°, respectively.

which is 80 km southeast of the weather radar in De Bilt. The geographical position of the bird tracking radar is indicated on the map in Fig. 1. The bird radar has a peak power of 160 kW and a pulse duration of 0.2 μs after pulse compression. The radar has a pencil beam antenna with a 3-dB width of 2.4° and a vertical scanning speed of 30° s^{-1}. Table 1 lists the relevant technical parameters of the bird tracking radar.

To obtain information on the bird migration intensity, range–height scans perpendicular to the main northeast direction of the spring migration were performed every half-hour between 3 March and 22 May 2003. From 16 April 2003 onward, the bird radar was not operational between 1000 and 1500 UTC for maintenance. The pencil beam scanned 60 times between 0° and 60° elevation during a 5-min period. An example of a range–height scan from the bird tracking radar is displayed in Fig. 3. The reflection layer at the top of the image, corresponding to an altitude of 5 km, is due to a cloud layer. The numerous distributed echoes at lower altitudes are attributed to scattering from (flocks of) birds.

The Radar Observation of Bird Intensity (ROBIN) processor (Buurma 1995; van Gasteren et al. 2008) is used to collect and analyze these range–height scans. The ROBIN system digitizes the analog signal from the receiver and optimizes the signal for bird detection by subtracting a sensitivity time control (STC) level (which corrects the signal for range) and a false alarm rate
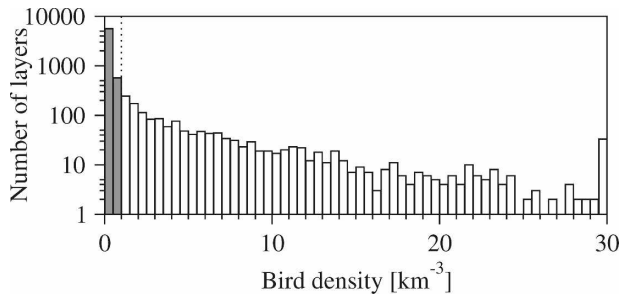
FIG. 4. Histogram of the number of time–height layers as a function of the bird migration density in 0.5 km^{-3} density bins. A threshold of 1.0 bird echo per km^3 is suggested for determining the presence (white bars) or absence (gray bars) of birds.

level (which optimizes the signal-to-noise ratio). Volume echoes due to precipitation and ground clutter are removed based on their strong reflectivity and intensity variances (high for precipitation and low for clutter). Subsequently, the bird "point" echoes in the individual scans (see Fig. 3) are identified using an intensity threshold and counted. Then the corrected bird densities are calculated from the number of birds and the estimated beam volume. An informative review of the technical basis for the study of bird migration by radar is given by Bruderer (1997a).

The X-band radar detects birds at ranges between 0.1 and 7 km from the antenna. Bird detection probability per pulse volume decreases for increasing ranges from the antenna due to decreasing signal strength and for decreasing ranges due to the small beam volume (Bruderer 1997a). In addition, strong clutter due to insects is often seen for ranges up to 2 km. Therefore,

only birds detected in the range between 2 and 4.5 km are used and an empirical correction for the loss of detection with range is applied (van Gasteren et al. 2008). Thus, the radar data from the range–height scans have been used to calculate bird densities for 200-m altitude layers between 0 and 4 km above ground level and for 3-h accumulation periods centered at 0000, 0300 UTC, and so on. The 3-h averaging windows ensure that sufficient observations are available and match the analysis times of the HIRLAM model. Bird density observations for 7700 time–height layers (385 profiles) have been obtained during the spring 2003 migration.

The bird density observations have been used to construct a histogram with the number of time–height layers for different bird densities (see Fig. 4). The histogram exhibits a large peak for bird densities below 1 km^{-3} and a long tail with densities exceeding 30 bird echoes per cubic kilometer. Note that bird densities higher than 30 km^{-3} are counted in the highest bin. Based on this histogram and in accordance with the optimum value found by van Gasteren et al. (2008), a threshold of 1.0 bird echo per cubic kilometer is selected for determining the presence or absence of birds using the bird tracking radar.

In the left frame of Fig. 5, a histogram of the number of time–height layers per day exceeding the 1.0 km^{-3} threshold is shown. Note that the total number of time–height layers per day is 160. The histogram bars represent the number of "bird" layers (i.e., layers with a mean bird echo density exceeding the threshold), as determined by the bird radar. The gray fillings represent the number of bird layers for which a corresponding weather radar wind vector is available. In most
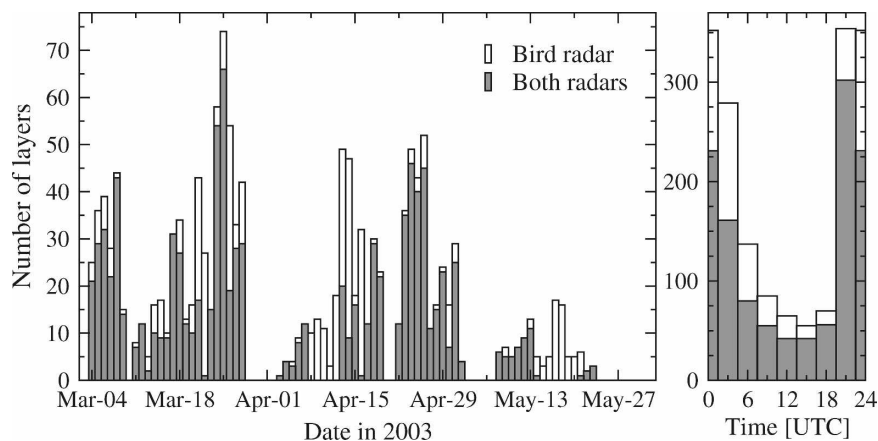

FIG. 5. Two histograms of the observed bird density using a 1-km^{-3} threshold are shown. (left) The number of time–height layers with birds as a function of date and (right) the same, as a function of time of day. The histogram bars represent the number of bird layers and the gray fillings the number that could be collocated with a "wind" observation from the Doppler weather radar.

cases the histogram bars are almost fully gray. White bars are due to missing weather radar data (14–20 May) and to local variations in the migration pattern. Only time–height layers with valid data from both radars are used in the comparison. Intense bird migration is observed in March and April, with a clear maximum on 24 March 2003. In March, broad-front bird migration over the Netherlands occurs generally from west (from the United Kingdom) to east, while in April and May it usually occurs from southwest (from Africa, Iberia, and France) to northeast. Because the coverages of both radars are not overlapping (80-km distance), the spatial homogeneity and temporal continuity of the broad-front bird migration are crucial for this comparison. More details of the spatial and temporal characteristics of the Palaeartic–African migration system are given in Bruderer (1997b).

Figure 5 (right panel) shows the diurnal cycle of the number of bird layers as observed by the bird radar only (histogram bars) and by both radars (gray fillings). The radar observations indicate that bird migration is most abundant between 1800 and 0600 UTC (i.e., approximately nighttime in local time). During daytime, birds tend to migrate in large groups and at low altitudes (below 100 m), while during nighttime they usually migrate in smaller groups (thus the same number of birds affects more radar volumes) and at altitudes up to 4 km (Bruderer 1997b). As a consequence, nocturnal migration is much better detected by a bird radar and (unfortunately) also by weather radars. The mean altitude distributions of all observed bird migration (histogram bars) and nighttime only (gray fillings) are presented in Fig. 6. The aforementioned differences in height distribution of the detected bird migration between day and night are evidently supported by this figure.

3. Results of comparison

The velocity observations from the weather radar have been combined with the bird density data from the bird tracking radar. The 3-h accumulations from the bird radar have been merged with the weather radar wind profiles observed halfway through the accumulation period. Bird and wind data from the lowest height layer (0–200 m) have been removed from the dataset because of residual sidelobe clutter contamination in the radar winds and the inhomogeneity of the bird migration at these low altitudes. Figure 7 shows a scatterplot of the radial velocity standard deviation σ_r [calculated according to Eq. (2)] versus the reflectivity for the weather radar wind vectors. In total, 2131 weather ra-
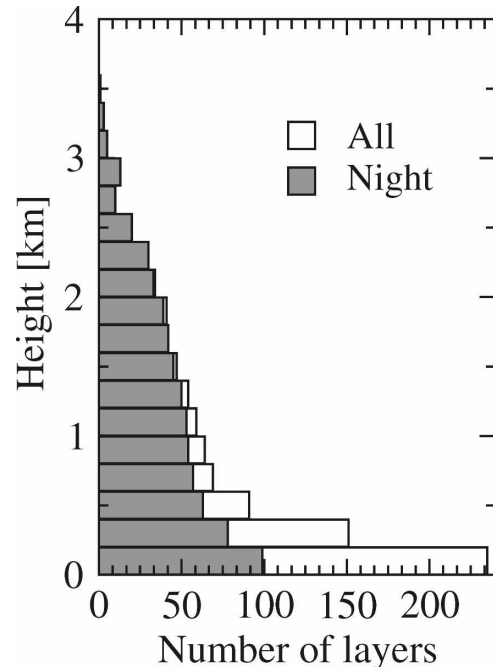

FIG. 6. The histogram displays the number of time–height layers with birds as a function of the height using a 1-km^{-3} threshold. The histogram bars represent the profile for all bird radar observations and the gray fillings represent the "nighttime" (1800–0600 UTC) profile only.

dar wind vectors were combined with simultaneous 3-hourly bird radar observations between 3 March and 22 May 2003. The bullets in the scatterplot are colored depending on the density of migrating birds as determined by the bird tracking radar. Most bullets are scattered below the horizontal line at 2 m s^{-1} and they correspond to good-quality wind vectors in clear-air (low reflectivity) or precipitation (reflectivity above 0 dBZ) cases. It is also evident from the figure that bird vectors [i.e., velocity vectors retrieved during dense bird migration (blue-to-red bullets)] have mostly a radial velocity standard deviation larger than 2 m s^{-1}. Wind vectors (purple bullets) with large standard deviation and low reflectivity are seen as well. To prevent rejection of wind vectors with large standard deviations in convective situations or frontal passages, one could additionally use a reflectivity threshold. Because the combination of reflectivity above 0 dBZ and $\sigma_r > 2$ m s^{-1} is rare in our dataset (see Fig. 7), such an additional threshold is not applied here.

The scatterplot in Fig. 7 can be analyzed quantitatively using so-called performance matrices or contingency tables. Two contingency tables for the weather radar vectors against the bird radar observations are presented in Table 2. The contingency table relates classified radar wind (columns) and bird (rows) obser-
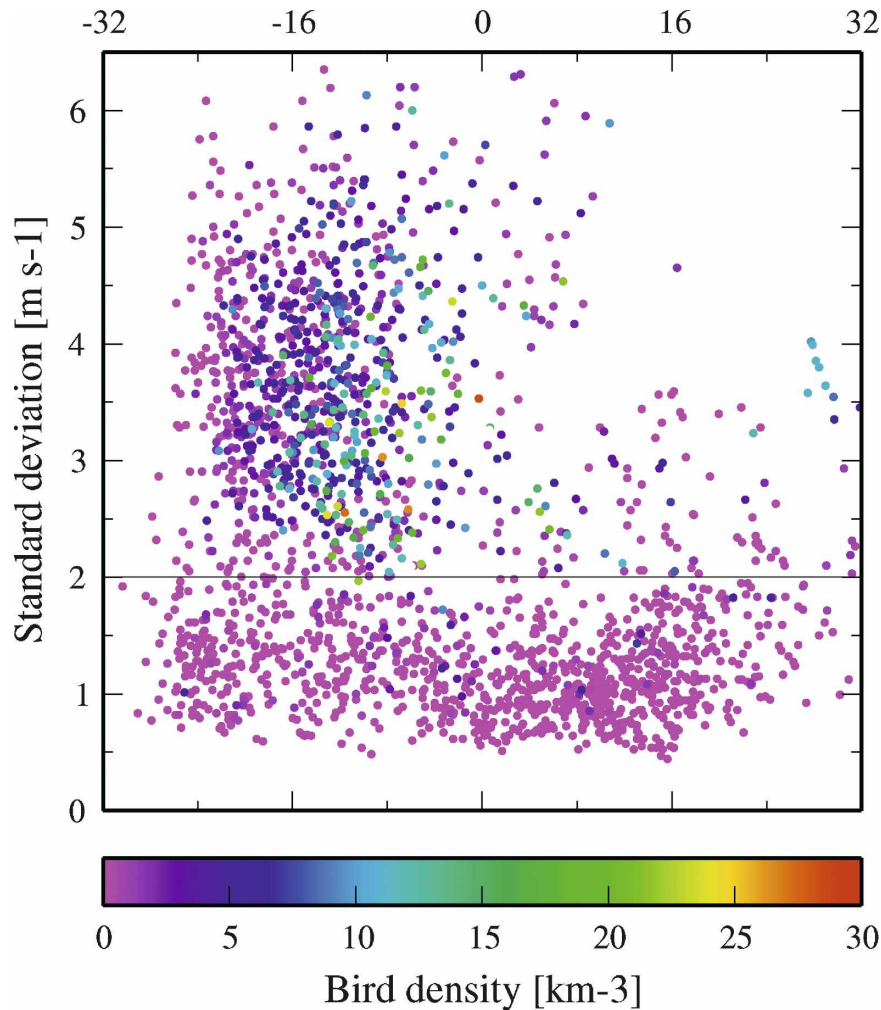
FIG. 7. A scatterplot of the reflectivity and radial velocity standard deviation (σ_r) for the weather radar wind vectors. The scattered bullets are colored according to the corresponding bird density observed by the bird tracking radar. The horizontal line marks the applied threshold for the operational wind profiles.

vations. A σ_r threshold of 2 m s^{-1} is used to classify the weather radar vectors into "wind" and "no wind." For the bird density data from the tracking radar a threshold of 1 km^{-3} is used to determine the presence or absence of birds. The four symbols in the lhs columns, H, M, F, and R, refer to the number of hits, misses, false alarms, and correct rejections, respectively. The rhs columns list the actual numbers for the 2131 weather radar wind vectors in the dataset. It is evident that the number of hits and the number of correct rejections are considerably larger than the two off-diagonal elements. The number of false alarms is relatively low indicating that after quality control only a few wind vectors are still contaminated by migrating birds. The wind vectors rejected by the quality control in absence of any bird echo are counted as misses. Figure 7 shows that these

wind vectors are derived from clear-air echoes (reflectivity below 0 dBZ). These clear-air weather radar echoes are probably due to insects (Wilson et al. 1994; Martin and Shapiro 2007).

Various statistical scores can be derived from a contingency table (Wilks 1995). The fraction correct (FC), probability of detection (POD), false alarm ratio

TABLE 2. Contingency table for the quality-controlled weather radar wind vectors against the bird radar observations. A standard deviation threshold of $\sigma_r = 2.0$ m s^{-1} and a bird density threshold of 1.0 km^{-3} have been applied.

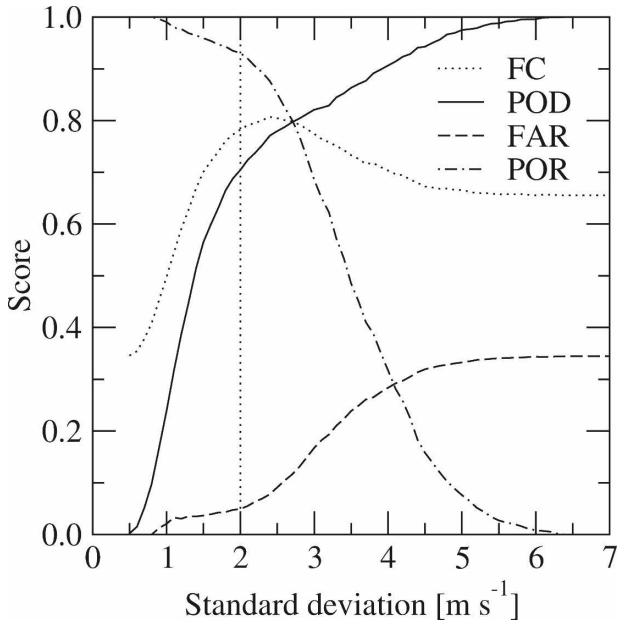| Wind	No wind		Wind	No wind
H	M	No birds	984	413
F	R	Birds	51	683

FIG. 8. FC, POD, FAR, and POR for detection of true wind vectors as a function of the applied threshold on the standard deviation (σ_r). These scores have been determined from the scatterplot of Fig. 7. The vertical dashed line marks the applied threshold for the operational wind profiles.
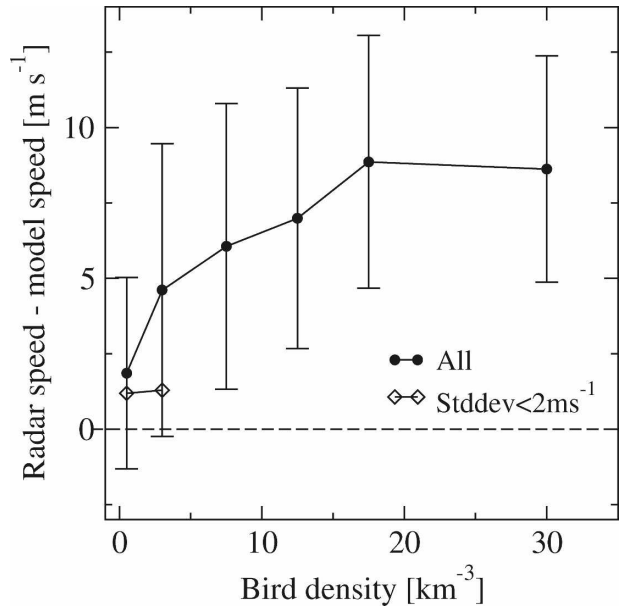

FIG. 9. Bias and standard deviation of the weather radar wind speeds against the NWP (HIRLAM) model wind speeds as a function of the observed bird density. Results for all data (●) and for quality-controlled wind profile data (◇) are given.

(FAR), and probability of rejection (POR) are calculated as follows:

$$FC \equiv \frac{H + R}{H + F + M + R} = 0.782, \quad (3)$$

$$POD \equiv \frac{H}{H + M} = 0.704, \quad (4)$$

$$FAR \equiv \frac{F}{H + F} = 0.049, \quad (5)$$

$$POR \equiv \frac{R}{R + F} = 0.931, \quad (6)$$

using the symbols and numbers in Table 2. Using a radial velocity standard deviation threshold of $\sigma_r = 2.0$ m s^{-1}, over 78% of the weather radar vectors are classified correctly (FC). POD reflects the fraction of wind vectors that are accepted correctly, and it suffers from the rejection of the clear-air vectors not related to birds (mostly due to insects). During this spring with several cases of broad-front migration (see Fig. 5), less than 5% of the quality-controlled (using the standard deviation threshold) wind vectors are potentially contaminated with migrating birds. Furthermore, one can see from the POR score that more than 93% of the bird vectors are rejected correctly.

Naturally, the standard deviation threshold σ_r can be

changed and contingency tables can be compiled for each threshold value. Figure 8 shows the derived statistical scores as a function of the radial velocity standard deviation threshold. It is evident that the performance of the quality control can be altered significantly by changing the standard deviation threshold. A σ_r threshold of 1 m s^{-1}, for instance, leads to a very stringent quality control with hardly any bird contamination (FAR = 0.02 and POR = 0.99) at the cost of a low fraction of accepted wind vectors (POD = 0.24). A relaxed quality control is obtained with a high threshold of, for example, $\sigma_r = 5$ m s^{-1}, where almost 98% of the wind vectors is accepted, yet a high degree of bird contamination is observed (FAR = 0.33). A default threshold of 2 m s^{-1} is proposed in Fig. 8 by the vertical dashed line, but the optimum σ_r threshold depends on the application.

Similarly to Holleman (2005), the horizontal wind speed data retrieved from the weather radar in De Bilt have been compared to those obtained from the operational HIRLAM model, which does not yet assimilate the weather radar wind profiles. The bird densities observed by the bird radar have been used to distribute the wind speed data over different bins. For each bin the bias and standard deviation of the weather radar and model wind speeds are calculated. The results for all wind data (●) for the quality-controlled wind data (◇) are displayed in Fig. 9. The default threshold of $\sigma_r = 2$ m s^{-1} has been applied. For all wind data, a gradual
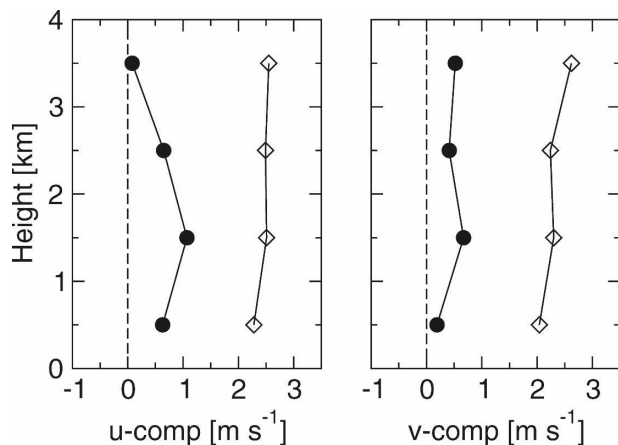
FIG. 10. Profiles of the bias (●) and standard deviation (◇) of the Cartesian u and v components from the verification of weather radar wind profiles against the HIRLAM model. A threshold of $\sigma_r = 2$ m s^{-1} has been used to quality control the radar wind data.

increase of the wind speed bias is observed for an increasing bird density. At high bird densities around 30 km^{-3}, the weather radar wind speeds have a significant positive bias of 8.6 ± 3.8 m s^{-1}. This observed bias is in good agreement with the typical airspeed of migrating birds, which ranges from 7 up to 20 m s^{-1} (Koistinen 2000), and the absolute velocity differences between VAD and radiosonde wind profiles (up to 12.9 m s^{-1}) as observed by Gauthreaux et al. (1998). For the quality-controlled wind vectors, a small positive speed bias (1 m s^{-1}) is observed, indicating that most bird-contaminated vectors have been rejected. This residual bias, which has been observed before, is due to the rejection of radial velocities close to zero during the wind profile retrieval (Holleman 2005). For moderate bird densities, between 1 and 5 km^{-3} (second point from left), the quality control reduces the speed bias by almost 4 m s^{-1} and for higher bird densities all wind vectors are rejected.

Figure 10 shows the bias (●) and standard deviation (◇) of the Cartesian u and v components of the retrieved wind profiles against the analyzed profiles from the HIRLAM model. All radar wind vectors have been quality controlled using a threshold of $\sigma_r = 2$ m s^{-1}. These so-called observation minus background statistics must be evaluated prior to assimilation of observations in an NWP model. The figure reveals a small positive bias (<1 m s^{-1}) for both Cartesian components. The standard deviation against the HIRLAM background of 2–2.5 m s^{-1} is in accordance with previous verification results (Holleman 2005). It is concluded that all (significant) bird contamination is removed from the weather radar wind data by the σ_r quality control. Moreover, this figure demonstrates that high-

quality weather radar wind profiles can be obtained, even during the bird migration season.

4. Conclusions

The quality of weather radar wind profiles can be degraded severely during bird migration. Detailed understanding of the bird contamination and development of appropriate quality-control procedures are prerequisites for routine assimilation of these wind profiles in NWP models. Here we presented a quality assessment of weather radar wind profiles during the spring migration of 2003. Operational wind profiles from the weather radar in De Bilt, in the center of the Netherlands, have been subjected to this assessment.

Data from a bird tracking radar have been used to assess the impact of bird migration on the weather radar wind profiles. This X-band radar was located about 80 km southeast of the weather radar. The bird radar performed range–height scans perpendicular to the main direction of the migration. Bird densities are deduced by counting and normalizing the observed echoes, and by subsequent correction for the range dependence of the detection efficiency. The peaks in the bird migration intensity between 3 March and 22 May 2003 are clearly recognized in the dataset. Furthermore, it was observed that nocturnal bird migration occurs at higher altitudes and therefore is much better detected by a (bird) radar than diurnal migration. Thus nocturnal bird migration can have a much larger (negative) impact on weather radar observations.

The comparison of the weather radar and bird radar data evidences that the radial velocity standard deviation σ_r obtained from the wind profile retrieval is a skillful indicator of bird contamination. This finding is in accordance with a previous observation by Koistinen (2000). A standard deviation threshold of $\sigma_r = 2.0$ m s^{-1} is proposed for the quality controlling of weather radar wind profiles, but the optimum threshold depends on the application (e.g., NWP assimilation or nowcasting). Therefore, supplying the radial velocity standard deviation data with the wind profiles is recommended so that users can set their own threshold. With the proposed threshold of 2.0 m s^{-1}, more than 93% of the contaminated wind vectors are rejected while over 70% of the wind vectors are accepted correctly. The 30% missed wind vectors were mainly derived from clear-air echoes, probably from insects.

The "wind–bird radar" comparison could be improved when the two radars have a smaller distance between them and thus data from spatially overlapping regions are analyzed. Furthermore, the bird rejection

algorithm could be extended with a variable standard deviation threshold by inclusion of criteria on reflectivity or signal-to-noise, and by considering the spectral width data from the Doppler weather radar. The identification and treatment of the other main cause of clear-air echoes, insects, is an important challenge. Polarimetric weather radar, which is rapidly becoming the operational standard, offers additional variables to separate wind, insects, and migrating birds (e.g., using multimodal spectra; Bachmann and Zrnić 2007). Dedicated measurement campaigns with a mobile bird tracking radar in the vicinity of polarimetric and Doppler weather radars are planned for 2008.

From the comparison with wind data from the operational HIRLAM model, it appears that the raw weather radar wind speeds have a positive bias of 8.6 ± 3.8 m s^{-1} during strong bird migration while the quality-controlled wind speeds have a negligible bias. The significant speed bias of the raw wind data is in good agreement with the typical airspeed of migrating birds (7–20 m s^{-1}) and observations by others (up to 12.9 m s^{-1}). The bias and standard deviation of the Cartesian components of the quality-controlled wind profiles have been determined against the HIRLAM background. From these observations minus background statistics it is concluded that all (significant) bird contamination is removed and that high-quality weather radar wind profiles are obtained during the bird migration season.

REFERENCES

Bachmann, S., and D. Zrnić, 2007: Spectral density of polarimetric variables separating biological scatterers in the VAD display. *J. Atmos. Oceanic Technol.,* **24,** 1186–1198.

Bouten, W., and Coauthors, 2003: Towards an operational bird avoidance system: Combining models and measurements. *Proc. 26th Int. Bird Strike Committee,* Warsaw, Poland, 19–31.

Browning, K. A., and R. Wexler, 1968: The determination of kinematic properties of a wind field using Doppler radar. *J. Appl. Meteor.,* **7,** 105–113.

Bruderer, B., 1997a: The study of bird migration by radar. Part I: The technical basis. *Naturwissenschaften,* **84,** 1–8.

——, 1997b: The study of bird migration by radar. Part II: Major achievements. *Naturwissenschaften,* **84,** 45–54.

Buurma, L. S., 1995: Long-range surveillance radars as indicators of bird numbers aloft. *Isr. J. Zool.,* **41,** 221–236.

Collins, W. G., 2001: The quality control of velocity azimuth display (VAD) winds at the National Centers for Environmental Prediction. Preprints, *11th Symp. on Meteorological Observations and Instrumentation,* Albuquerque, NM, Amer. Meteor. Soc., 9.2.

Crook, N. A., and J. Sun, 2004: Analysis and forecasting of the low-level wind during the Sydney 2000 Forecast Demonstration Project. *Wea. Forecasting,* **19,** 151–167.

Gauthreaux, S. A., Jr., and C. G. Belser, 1998: Displays of bird movements on the WSR-88D: Patterns and quantification. *Wea. Forecasting,* **13,** 453–464.

——, D. S. Mizrahi, and C. G. Belser, 1998: Bird migration and bias of WSR-88D wind estimates. *Wea. Forecasting,* **13,** 465–481.

Gematronik, 2003: Rainbow 3.4 operator's manual. Gematronik, 215 pp.

Holleman, I., 2005: Quality control and verification of weather radar wind profiles. *J. Atmos. Oceanic Technol.,* **22,** 1541–1550.

——, and H. Beekhuis, 2003: Analysis and correction of dual-PRF velocity data. *J. Atmos. Oceanic Technol.,* **20,** 443–453.

Koistinen, J., 2000: Bird migration patterns on weather radars. *Phys. Chem. Earth,* **25B,** 1185–1194.

Lhermitte, R. M., and D. Atlas, 1961: Precipitation motion by pulse Doppler radar. Preprints, *9th Conf. on Radar Meteorology,* Kansas City, MO, Amer. Meteor. Soc., 218–223.

Lindskog, M., K. Salonen, H. Järvinen, and D. B. Michelson, 2004: Doppler radar wind data assimilation with HIRLAM 3DVAR. *Mon. Wea. Rev.,* **132,** 1081–1092.

Liu, S., Q. Xu, and P. Zhang, 2005: Identifying Doppler velocity contamination caused by migrating birds. Part II: Bayes identification and probability tests. *J. Atmos. Oceanic Technol.,* **22,** 1114–1121.

Martin, W. J., and A. Shapiro, 2007: Discrimination of bird and insect radar echoes in clear air using high-resolution radars. *J. Atmos. Oceanic Technol.,* **24,** 1215–1230.

Michelson, S. A., and N. L. Seaman, 2000: Assimilation of NEXRAD-VAD winds in summertime meteorological simulations over the northeastern United States. *J. Appl. Meteor.,* **39,** 367–383.

Parrett, C. A., M. Turp, B. Macpherson, and T. Oakley, 2004: Quality monitoring of weather radar wind profiles at the Met Office. *ERAD Pub. Series,* **2,** 168–173.

Press, W. H., S. A. Teukolsky, W. T. Vetterling, and B. P. Flannery, 1992: *Numerical Recipes in C: The Art of Scientific Computing.* 2nd ed. Cambridge University Press, 994 pp.

Rinne, J., 2000: The use of radar wind observations in numerical assimilation. *Phys. Chem. Earth,* **25B,** 1273–1276.

Shamoun-Baranes, J., E. van Loon, H. van Gasteren, J. van Belle, W. Bouten, and L. Buurma, 2006: A comparative analysis of the influence of weather on the flight altitudes of birds. *Bull. Amer. Meteor. Soc.,* **87,** 47–61.

Sigmet, 1998: RVP6 Doppler Signal Processor user's manual. Sigmet Inc., 208 pp.

Sirmans, D., D. Zrnić, and B. Bumgarner, 1976: Extension of maximum unambiguous Doppler velocity by use of two sampling rates. Preprints, *17th Conf. on Radar Meteorology,* Seattle, WA, Amer. Meteor. Soc., 23–28.

Sun, J., and N. A. Crook, 2001: Real-time low-level wind and temperature analysis using single WSR-88D data. *Wea. Forecasting,* **16,** 117–132.

Unden, P., and Coauthors, 2002: HIRLAM-5 scientific documentation. Tech. Rep. HIRLAM-5 Project, SMHI, 146 pp.

van Gasteren, H., I. Holleman, W. Bouten, E. van Loon, and J. Shamoun-Baranes, 2008: Extracting bird migration information from C-band weather radars. *Ibis,* **150,** 674–686.

Waldteufel, P., and H. Corbin, 1979: On the analysis of single Doppler radar data. *J. Appl. Meteor.,* **18,** 532–542.

Wilks, D. S., 1995: *Statistical Methods in the Atmospheric Sciences.* Academic Press, 467 pp.

Wilson, J. W., T. M. Weckwerth, J. Vivekanandan, R. M. Wakimoto, and R. W. Russell, 1994: Boundary layer clear-air radar echoes: Origin of echoes and accuracy of derived winds. *J. Atmos. Oceanic Technol.,* **11,** 1184–1206.

Zhang, P., S. Liu, and Q. Xu, 2005: Identifying doppler velocity contamination caused by migrating birds. Part I: Feature extraction and quantification. *J. Atmos. Oceanic Technol.,* **22,** 1105–1113.

Zhao, Q., J. Cook, Q. Xu, and P. R. Harasti, 2006: Using radar wind observations to improve mesoscale numerical weather prediction. *Wea. Forecasting,* **21,** 502–522.